Multimodal gradients across mouse cortex

Ben D. Fulcher[a,1], John D. Murray[b], Valerio Zerbi[c], and Xiao-Jing Wang[d,e,1]

[a]School of Physics, Sydney University, Sydney, NSW 2006, Australia; [b]Department of Psychiatry, Yale University School of Medicine, New Haven, CT 06511; [c]Neural Control of Movement Laboratory, Department of Health Sciences and Technology, Eidgenössische Technische Hochschule Zürich, 8057 Zürich, Switzerland; [d]Center for Neural Science, New York University, New York, NY 10003; and [e]Shanghai Research Center for Brain Science and Brain-Inspired Intelligence, Shanghai 201210, China

Edited by Robert Desimone, Massachusetts Institute of Technology, Cambridge, MA, and approved January 22, 2019 (received for review August 16, 2018)

The primate cerebral cortex displays a hierarchy that extends from primary sensorimotor to association areas, supporting increasingly integrated function underpinned by a gradient of heterogeneity in the brain's microcircuits. The extent to which these hierarchical gradients are unique to primate or may reflect a conserved mammalian principle of brain organization remains unknown. Here we report the topographic similarity of large-scale gradients in cytoarchitecture, gene expression, interneuron cell densities, and long-range axonal connectivity, which vary from primary sensory to prefrontal areas of mouse cortex, highlighting an underappreciated spatial dimension of mouse cortical specialization. Using the T1-weighted:T2-weighted (T1w:T2w) magnetic resonance imaging map as a common spatial reference for comparison across species, we report interspecies agreement in a range of large-scale cortical gradients, including a significant correspondence between gene transcriptional maps in mouse cortex with their human orthologs in human cortex, as well as notable interspecies differences. Our results support the view of systematic structural variation across cortical areas as a core organizational principle that may underlie hierarchical specialization in mammalian brains.

cortical hierarchy | gene expression | cortical gradients | interspecies comparison

Across the brain, cortical microcircuits vary in their cytoarchitecture (1–3); myeloarchitecture (3–5); dendritic and synaptic structure (6–13); and the size, density, and laminar distribution of distinct cell types (1, 3, 14–16). Many of these microstructural properties vary across the cortex continuously as spatial gradients (1–3, 17–20) that shape the specialized functional capabilities of different cortical areas (7), through variations in plasticity (5), inhibitory control (21), and electrophysiological properties (6, 10). Prominent gradients follow a hierarchy of increasing functional integration, from primary sensory to transmodal association areas in primate cortex, pointing to their role in shaping functional specialization along the cortical hierarchy (22–25). The mouse cortex is relatively uniform compared with the highly differentiated primate cortex (10, 26–28), but recent evidence has nevertheless pointed to a global hierarchy of mouse cortical areas (29, 30). It remains unknown whether the hierarchical gradients of primate cortex exist and play a similar role in functional specialization in the mouse and may therefore represent a conserved property of mammalian brain organization.

The mouse is an ideal model to investigate gradients of cortical microstructure, with experimental datasets from diverse modalities available in standardized anatomical reference spaces (31). Cortical maps of a wide range of properties, many of which are unavailable in humans, have been measured in mice, including (*i*) gene expression with approximate genome-wide coverage (32), (*ii*) interneuron cell densities (29), (*iii*) tract-traced axonal connectivity (30, 33–36), (*iv*) cytoarchitecture (37), (*v*) cell/neuron density (38–40), and (*vi*) resting-state function magnetic resonance imaging (fMRI) (41–43). Existing work has demonstrated an association between pairs of these measurements (42–44), but these data have not previously been characterized together from the viewpoint of macroscopic gradients.

The ratio of T1-weighted to T2-weighted (T1w:T2w) images is a noninvasive MRI measurement that has been measured in mice, macaques, and humans, providing a common spatial reference map for linking large-scale cortical gradients across species. Commonly interpreted as a marker of intracortical myelin content (45), T1w:T2w is also sensitive to a wide range of other microstructural properties (46). In macaque cortex, T1w:T2w is strongly correlated to the established structural hierarchy of feedforward–feedback interareal laminar projections (47), and in human cortex it follows dominant gene transcriptional gradients, positioning it as a strong candidate marker of hierarchical specialization (25). Here we show that gradients of diverse properties of mouse cortex exhibit a common spatial patterning along a candidate functional hierarchy. We use T1w:T2w as a common spatial reference to demonstrate a correspondence of gradients of cytoarchitecture between mice, macaques, and humans and with transcriptional maps of ortholog genes between mice and humans. Our results reveal an interspecies conservation of cortical gradients that may shape the functional specialization of mammalian cortical circuits, consistent with systematic structural variation across cortical areas as a core organizing principle (48).

Results

We analyzed the spatial maps of diverse cortical properties across 40 areas of the Allen Reference Atlas (ARA) (49), shown in Fig. 1 *A* and *B*. The similarity between two spatial maps was quantified as the Spearman rank correlation coefficient, ρ, across as many cortical areas as could be matched between a given pair of modalities (40 unless otherwise specified). Corrected P values, P_{corr}, are calculated using the method of Benjamini and Hochberg (50).

Significance

The brain is organized into processing streams, along which incoming sensory information is processed at increasingly abstract and integrative levels. This specialization of function is thought to be underpinned by corresponding changes in the brain's local circuitry. Here we combine a wide range of measurements across the mouse brain, including the expression of genes, cell densities, and axonal connectivity, to show that the properties of local circuits of the mouse brain vary along putative processing streams in a similar way to the primate brain. This similarity across species points to common mechanisms through which mammalian brains may process information.

Author contributions: B.D.F., J.D.M., and X.-J.W. designed research; B.D.F. and V.Z. performed research; J.D.M. and X.-J.W. contributed new reagents/analytic tools; B.D.F. and V.Z. analyzed data; and B.D.F., J.D.M., and X.-J.W. wrote the paper.

The authors declare no conflict of interest.

This article is a PNAS Direct Submission.

[1]To whom correspondence may be addressed. Email: ben.fulcher@sydney.edu.au or xjwang@nyu.edu.

This article contains supporting information online at www.pnas.org/lookup/suppl/doi:10.1073/pnas.1814144116/-/DCSupplemental.

Published online February 19, 2019.

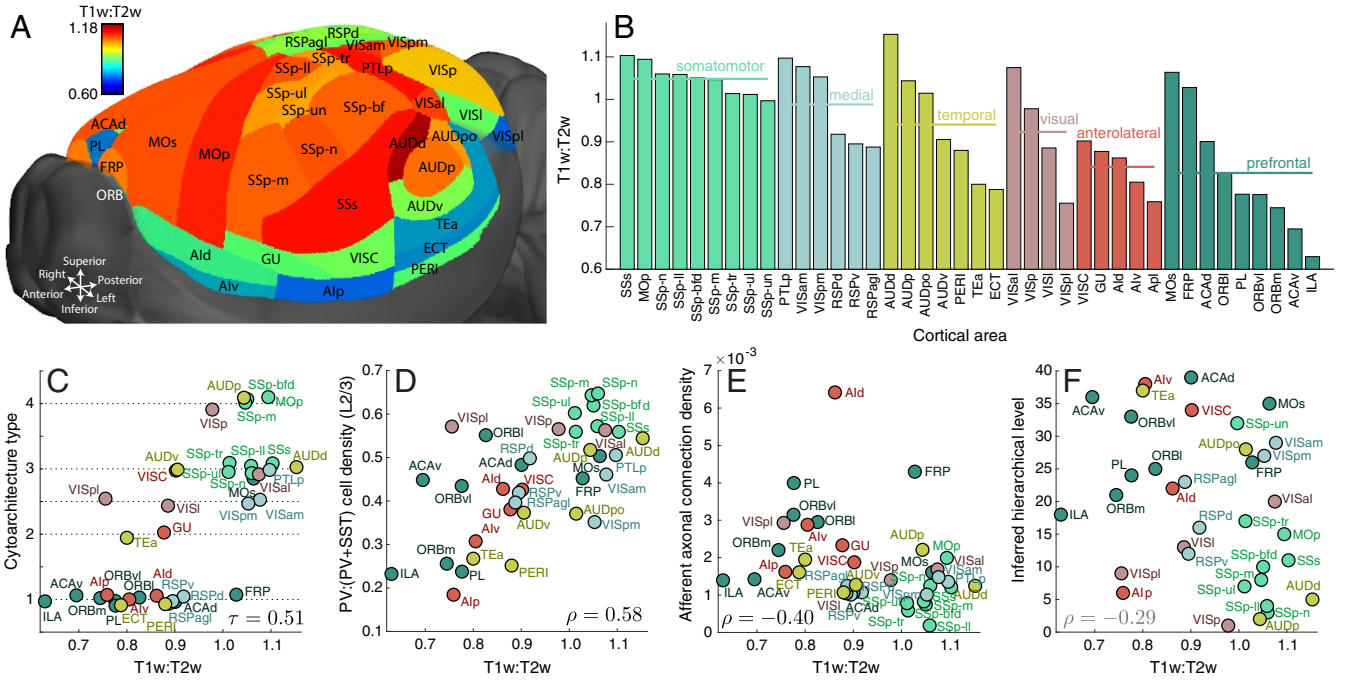

Fig. 1. The spatial map of the MRI measurement, T1w:T2w, is correlated with spatial maps of other structural properties. (*A*) Variation in T1w:T2w across mouse cortical areas (visualization through medial sections is in *SI Appendix*, Fig. S3). (*B*) T1w:T2w broadly decreases across families of connectivity-based groupings of cortical areas (30), from somatomotor areas to anterolateral and prefrontal areas. Groups are ordered by decreasing T1w:T2w, as are areas within each group. (*C*–*F*) Scatter plots are shown for T1w:T2w (horizontal axis) vs. (*C*) cytoarchitecture type (37), (*D*) relative density of PV(PV + SST) cells in L2/3 (29), (*E*) sum of incoming interareal axonal projection weight (33), and (*F*) hierarchical level inferred from feedforward–feedback laminar projection patterns (30). Circles are colored according to the connectivity modules in *B* and have sizes scaled by T1w:T2w. A small amount of vertical noise has been added to points in *C* to aid visualization (cytoarchitecture type takes discrete values, indicated as dotted horizontal lines). Abbreviations for cortical areas are defined in *SI Appendix*.

Cortical Gradients Follow T1w:T2w. We first investigated whether the T1w:T2w map is informative of functionally relevant macroscopic gradients of cortical variation in mice, as in macaques and humans (25). As shown in Fig. 1*A*, the T1w:T2w map of the mouse cortex displays nontrivial anatomical specificity on top of a broad spatial embedding, increasing along the inferior–superior axis, $|\rho| = 0.53$ ($P = 5 \times 10^{-4}$), perhaps in part reflecting a neurodevelopmental gradient of cortical maturation (51) (see *SI Appendix* for more details). Fig. 1*B* shows that T1w:T2w broadly decreases across five spatially localized connectivity modules (30), from somatomotor to prefrontal areas, consistent with a decreasing trend from primary unimodal to transmodal areas in macaques and humans (25). T1w:T2w is not significantly correlated to variation in cell density, $\rho = 0.21$ ($P = 0.2$) (39), or neuron density, $\rho = -0.08$ ($P = 0.6$, across 39 matching cortical areas) (40), making it well positioned to capture density-independent differences in neural architecture (1) (alternative data sources gave consistent results; *SI Appendix*).

Intracortical myelin, which T1w:T2w is sensitive to (45), increases with laminar differentiation (4, 5), with areas lower in the cortical hierarchy exhibiting a greater degree of laminar elaboration (22). Accordingly, T1w:T2w captures the variation in cytoarchitecture in macaques, Kendall's $\tau = 0.87$ (across eight cytoarchitectonic types), and humans, $\rho = 0.74$ (using layer IV gene markers) (25). As shown in Fig. 1*C*, we report a similar trend in mouse cortex, with T1w:T2w increasing from dysgranular to eulaminar areas, Kendall's $\tau = 0.51$ [$P = 2 \times 10^{-6}$, using five cytoarchitectonic categories assigned to 38 matching cortical areas (37)].

Interneuron densities vary across mouse cortical areas (29). In layer 2/3, sensory-motor areas contain a greater proportion of parvalbumin (PV)-containing interneurons, while association and frontal areas contain a greater proportion of somatostatin (SST)-containing interneurons; the ratio $\mathrm{PV} : (\mathrm{PV} + \mathrm{SST})$ orders cortical areas along a candidate functional hierarchy (29). We computed the correlation between T1w:T2w and layer 2/3 density of each of three measured interneuron cell types, PV-, SST-, and vasoactive intestinal peptide (VIP)-containing cells, as well as the proposed hierarchy marker, PV:(PV + SST) (29), across 36 matching cortical areas. PV:(PV + SST) is positively correlated with T1w:T2w, $\rho = 0.58$ ($P_{\mathrm{corr}} = 5 \times 10^{-4}$, correcting for four independent comparisons), as shown in Fig. 1*D*. The result is consistent with existing studies that have found a covariation of PV neuron density with myelin content (5) and the degree of laminar differentiation (15), leading to a characteristic variation of inhibitory control (2, 7, 48). Given a loose interpretation of SST interneurons as having a putative "input-modulating" function relative to the more "output-modulating" PV interneurons (29), this trend is also consistent with more functionally integrative areas (lower T1w:T2w) requiring greater input control. We also compared the interareal variation of T1w:T2w to cell densities (mm^{-3}) reported by Erö et al. (40) for glia, excitatory cells, inhibitory cells, modulatory cells, astrocytes, oligodendrocytes, and microglia across 39 matching cortical areas. We found a significant correlation between T1w:T2w and the density of glia, $\rho = 0.48$ ($P_{\mathrm{corr}} = 0.01$); inhibitory cells, $\rho = -0.47$ ($P_{\mathrm{corr}} = 0.01$); microglia, $\rho = 0.37$ ($P_{\mathrm{corr}} = 0.04$); and oligodendrocytes, $\rho = 0.37$ ($P_{\mathrm{corr}} = 0.04$) (scatter plots shown in *SI Appendix*, Fig. S6).

We next investigated whether T1w:T2w is related to properties of interareal axonal connectivity, measured using viral tract tracing (33), focusing on the normalized axonal connection density projected to (weighted in-degree, k^w_{in}) and from (weighted out-degree, k^w_{out}) each cortical area. Across 38 matching areas, T1w:T2w is significantly correlated with k^w_{in}, $\rho = -0.40$ ($P_{\mathrm{corr}} = 0.03$, correcting for two independent comparisons),

plotted in Fig. 1*E*, but not with k^{w}_{out}, $\rho = 0.14$ ($P_{\text{corr}} = 0.4$). This trend reflects a greater aggregate strength of axonal inputs in more functionally integrative areas (with lower T1w:T2w).

Comprehensive data on laminar-specific intracortical projection patterns have recently been used to assign candidate hierarchical levels to mouse cortical areas (30). The mouse cortex does not fit neatly into a global structural hierarchy, with a hierarchy score of just 0.126 (where 0 is nonhierarchical and 1 is perfectly hierarchical) (30). Here we found a weak negative correlation between T1w:T2w and hierarchical level in mice $\rho = -0.29$ ($P = 0.09$), as shown in Fig. 1*F*, in contrast to the strong negative correlation reported in macaques, $\rho = -0.76$ (25).

Gene Transcription. Gene transcriptional maps of the mouse brain, measured with cellular resolution using in situ hybridization, form the Allen Mouse Brain Atlas (AMBA) (32). We developed and applied stringent quality criteria to obtain cortical expression maps for 4,181 genes (listed in *SI Appendix*). We first focus on a selected set of 86 receptor subunit and cell-type marker genes (54) (*SI Appendix*). After correcting for testing multiple independent hypotheses (50) (a conservative correction due to the high intercorrelation between many of these genes), we found that the transcriptional maps of 24 genes are significantly correlated with T1w:T2w ($P_{\text{corr}} < 0.05$, $|\rho| \geq 0.39$), including glutamate receptor subunits (*Grin3a*, *Grin2d*, *Grik1*, *Grik2*, *Grik4*, *Grm2*, *Grm5*); serotonin receptor subunits (*Htr1a*, *Htr2c*, and *Htr5b*); interneuron cell-type markers (*Pvalb* and *Calb2*); the myelin marker, *Mobp*; and a range of other receptor subunit genes, *Trhr*, *Mc4r*, *Chrm5*, *Galr2*, *Hcrtr2*, *Hcrtr1*, *P2ry12*, *P2ry14*, *Cnr1*, *Oxtr*, and *P2ry2* (see *SI Appendix*, Table S2 for full results). Correlation coefficients between T1w:T2w and transcriptional levels of a selected subset of glutamate receptor subunit and interneuron marker genes are plotted in Fig. 2*A*. The strong negative correlation between T1w:T2w and *Grin3a* expression, $\rho = -0.63$ ($P_{\text{corr}} = 5 \times 10^{-4}$), is shown in Fig. 2*B*.

To understand how T1w:T2w relates to dominant transcriptional gradients of a set of 1,055 brain-expressed genes (52), we used principal components analysis (PCA) to estimate the most explanatory spatial maps of transcriptional variation (accounting for missing values using probabilistic PCA (55); *SI Appendix*). The first PC of cortical transcription is significantly correlated with the T1w:T2w map, $|\rho| = 0.53$ ($P = 6 \times 10^{-4}$), as it is in human cortex, $|\rho| = 0.81$ (25) (the correlation with PC2 is weaker, $|\rho| = 0.29$; compare with *SI Appendix*, Fig. S4). Fig. 2*C* displays a projection of cortical areas into the space of the two leading PCs, placing areas with similar transcriptional profiles close to one another. This transcriptional organization of cortical areas clearly separates different functional processing streams and visually resembles parallel primary–transmodal hierarchies (22) that have recently been characterized in human resting-state fMRI (18).

Laminar Specificity. Are large-scale cortical gradients driven by the specialization of specific cortical layers? We investigated this question using layer-specific maps of gene transcription (32) and interneuron density (29). T1w:T2w was estimated for each brain area by combining all cortical layers (values of T1w:T2w computed in layers 1–5 were highly correlated to this overall measurement; *SI Appendix*, Fig. S5).

We first computed Spearman correlation coefficients, ρ, between T1w:T2w and cell densities of three types of interneurons (29) in each of five cortical layers: 1 (37 areas), 2/3 (37 areas), 4 (21 areas), 5 (36 areas), and 6 (35 areas). Results are plotted in Fig. 3*A* for each cortical layer (row) and cell type (column). Correcting across 15 (assumed independent) hypothesis tests (50)—each cell type in each cortical layer—we found a significant positive correlation between T1w:T2w and PV cell density in layer 5, $\rho = 0.52$ ($P_{\text{corr}} = 7 \times 10^{-3}$), and a negative correlation of SST cell density with T1w:T2w in layer 2/3, $\rho = -0.62$ ($P_{\text{corr}} = 4 \times 10^{-4}$) and layer 6, $\rho = -0.65$ ($P_{\text{corr}} = 4 \times 10^{-4}$). VIP cell density did not exhibit a significant correlation to T1w:T2w in any individual cortical layer.

We next investigated gene-expression patterns in cortical layers 1, 2/3, 4, 5, 6a, and 6b (32) across the 24 genes identified above to be significantly correlated to T1w:T2w, shown in Fig. 3*B* (results for all 86 genes are in *SI Appendix*, Fig. S7). Consistent with *Pvalb* expression as a marker of PV cell density, the two measurements exhibit a similar laminar pattern of T1w:T2w correlations (with the strongest correlation in layer 5, compare Fig. 3*A*) and a high overall correlation ($\rho = 0.82$; *SI Appendix*). For a given gene, the direction of correlation between its expression and T1w:T2w is mostly consistent across cortical layers. Some genes display an association with T1w:T2w in all individual layers (e.g., *Trhr*, *Grin3a*, and *Htr2c*), while other genes show an overall correlation with T1w:T2w that is restricted to specific cortical layers (e.g., the positive correlation with *Mobp* is driven by layer 4 and infragranular layers). These cell-density and gene-expression results demonstrate that macroscopic gradients of areal specialization are not

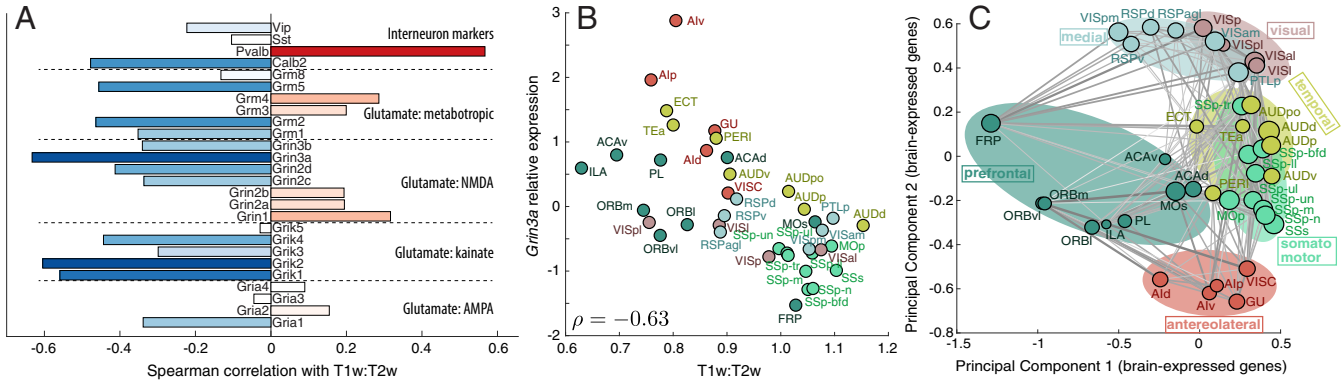

Fig. 2. Transcriptional maps of glutamate receptor subunit and interneuron marker genes covary with the T1w:T2w map, and a principal components projection of cortical areas using their gene expression profiles organizes them into meaningful processing streams. (*A*) Spearman correlation coefficients, ρ, between T1w:T2w and the transcriptional maps of genes coding glutamate receptor subunits and interneuron cell-type markers. (*B*) Scatter plot of T1w:T2w vs. *z*-score normalized levels of *Grin3a* transcription, $\rho = -0.63$ ($P_{\text{corr}} = 5 \times 10^{-4}$). (*C*) Projection of brain areas into the space of the two leading principal components of 1,055 brain-expressed genes (52) places cortical areas with similar transcriptional profiles close in the space, yielding a functionally informative organization of cortical areas. Brain areas are shown as circles with radii scaled by T1w:T2w and (symmetrized) axonal projections (33) are annotated where possible. Background shading has been added manually to guide the eye. Abbreviations for cortical areas are defined in *SI Appendix*.

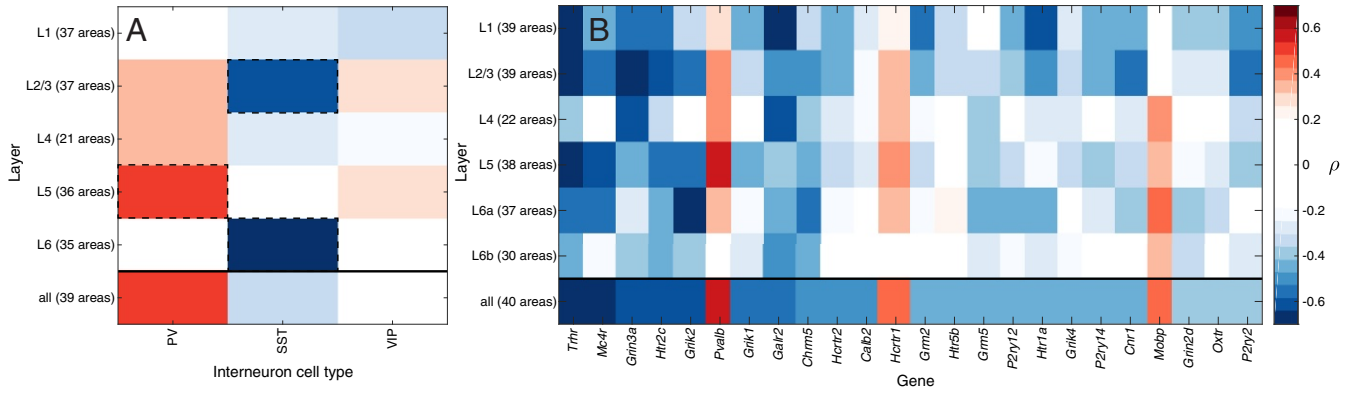

Fig. 3. Cell densities and gene expression exhibit distinctive laminar patterns of covariation with T1w:T2w across the mouse cortex. (*A* and *B*) Spearman correlation coefficients, ρ, of T1w:T2w are plotted as colors for (*A*) cell density of three types of interneurons (29) and (*B*) transcriptional level of a given gene (column) in a given cortical layer (row). Overall correlations, obtained from combining all layers of each area, are shown in the bottom row of each plot. Transcriptional levels (32) are shown for the 24 genes with significant overall correlations to T1w:T2w, ordered by their overall correlation to T1w:T2w (results for all 86 brain-related genes are in *SI Appendix*, Fig. S7).

dominated by particular cortical layers; all layers exhibit macroscopic gradients of areal specialization, for distinct microcircuit properties.

A Common Hierarchical Gradient. The variation of T1w:T2w mirrors the large-scale variation of microstructural properties along a putative functional hierarchy of cortical areas. To more directly understand relationships between the diverse cortical gradients characterized above, we combined representative measurements from each data type: gene expression, intracortical axonal connectivity, T1w:T2w, and interneuron cell density. These properties were visualized together by plotting the cortical variation of each measurement type with a distinct color map, as shown in Fig. 4. Measurements (columns) with highly correlated variation across cortical areas (rows) were placed close to each other using linkage clustering (*SI Appendix*). A common gradient emerges from the covariation of these diverse measurements of cortical structure, estimated as the first principal component of the data

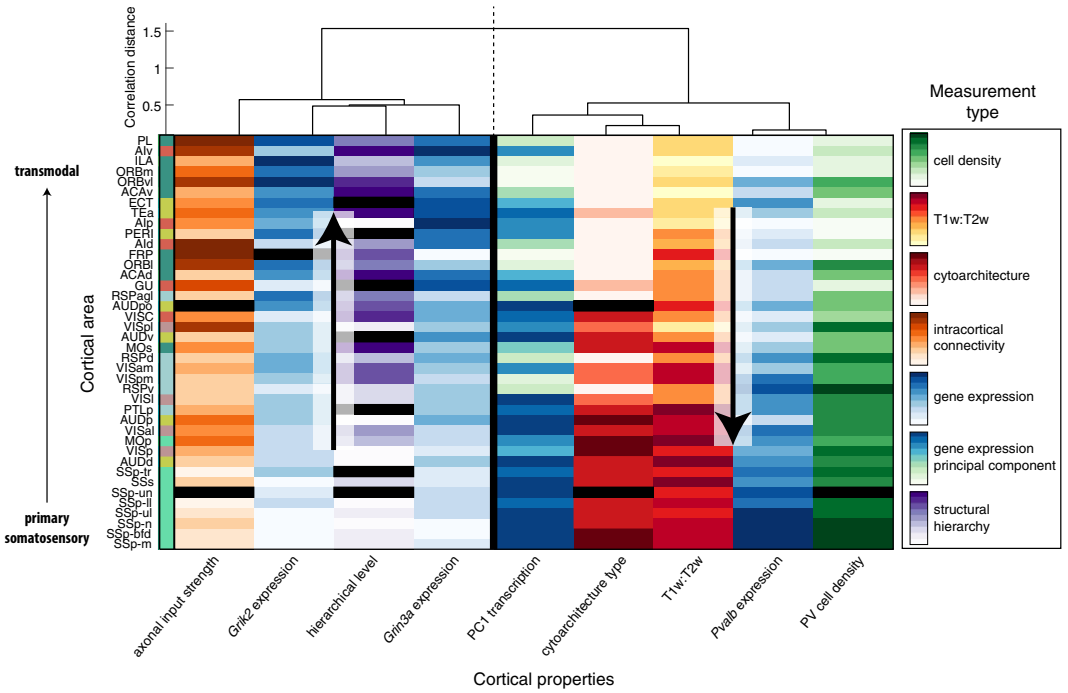

Fig. 4. Diverse measurements of cortical areas share a common gradient of variation. Cortical areas form rows, and measurements form columns, with different color maps used to code different datasets (from low values, light colors, to high values, dark colors), as labeled: density of PV neurons (29) (green); T1w:T2w (53) (yellow/red); cytoarchitecture (37) (red); weighted in-degree, k^w, of normalized axonal projection density (33) (orange); expression of three selected genes *Grin3a*, *Grik2*, and *Pvalb* (32) (blue); and the first principal component of brain-related genes (green-blue) and estimated hierarchical level (30) (purple). Areas (rows) are ordered according to the first principal component of this multimodal matrix of cortical properties and are colored according to their membership in one of six connectivity-based groupings (30) (compare with Fig. 1*B*). Measurements (columns) are ordered according to average linkage clustering on correlation distances according to the annotated dendrogram. Measurements cluster into two groups that either increase (*Left* cluster) or decrease (*Right* cluster) along a candidate functional hierarchy, from primary somatosensory to transmodal prefrontal areas. Missing data are shown as black rectangles.

and used to reorder the rows of Fig. 4. This consensus gradient orders areas along a putative functional hierarchy, from primary somatosensory to integrative prefrontal areas. Each individual measurement either increases or decreases along this consensus gradient, forming the two anticorrelated clusters shown in Fig. 4.

To investigate whether ordering areas by T1w:T2w or the structural hierarchical ordering of Harris et al. (30) better explains the multimodal cortical gradients, we compared how each correlates with the properties shown in Fig. 4 (across the 35 cortical areas common to both measurements). Spearman correlation coefficients were similar in magnitude between T1w:T2w and hierarchical level, and all properties but one (PV cell density) were more strongly correlated with T1w:T2w than with hierarchical level (*SI Appendix*, Fig. S8).

Mouse–Human Consistency Between T1w:T2w and Gene Transcriptional Gradients. T1w:T2w follows dominant transcriptional gradients in mouse and human cortex (25), but are the gradients of specific brain-related genes conserved between the two species? To investigate this, we compared the correlation between T1w:T2w and the transcription map of a given gene in mouse cortex, ρ_m, and for the human ortholog of that gene in human cortex, ρ_h (25), repeating the calculation for 70 of our 86 brain-related genes analyzed that have human orthologs and could be matched between the two datasets. Interspecies consistency in transcriptional gradients is reflected by a correspondence between the independent measurements of ρ_m and ρ_h, which we measured as a correlation across genes as ρ_{mh}. Although we have been careful to develop and apply rigorous quality-control criteria, the AMBA (32) and Allen Human Brain Atlas (AHBA) (56) can be noisy at the level of individual experiments; consequently, weak correlations with T1w:T2w in either humans (low ρ_h) or mice (low ρ_m) should not be interpreted as an absence of a relationship as much as strong correlations can be interpreted as evidence for a relationship.

As shown in Fig. 5, we find significant interspecies correspondence, $\rho_{mh} = 0.44$ ($P = 1 \times 10^{-4}$). The agreement is striking given measurement noise, vast differences in spatial scale, and distinct measurement modalities between mice (high-throughput in situ hybridization) and humans (postmortem microarray from six adults). Two of the genes with the strongest correlations with T1w:T2w in mouse cortex exhibit a similar variation in human cortex: *Grin3a*/*GRIN3A* ($\rho_m = -0.63$, $\rho_h = -0.65$) and *Pvalb*/*PVALB* $(0.57, 0.70)$. A range of other key genes exhibit strong interspecies consistency, including the interneuron marker *Calb2* $(-0.48, -0.45)$; the oxytosin receptor gene, *Oxtr* $(-0.41, -0.48)$; glutamate receptor genes *Grik1* $(-0.56, -0.54)$, *Grik2* $(-0.60, -0.52)$, and *Grik4* $(-0.44, -0.33)$; and myelin marker genes *Mobp* $(0.43, 0.41)$ and *Mbp* $(0.34, 0.45)$. Significant mouse–human correspondence was not limited to the brain-related genes shown in Fig. 5, but was reproduced for (*i*) all 2,951 genes, $\rho_{mh} = 0.25$ ($P = 8 \times 10^{-42}$); (*ii*) 806 brain-expressed genes (52), $\rho_{mh} = 0.31$ ($P = 2 \times 10^{-19}$); (*iii*) 60 astrocyte-enriched genes, $\rho_{mh} = 0.38$ ($P = 3 \times 10^{-3}$); (*iv*) 143 neuron-enriched genes, $\rho_{mh} = 0.40$ ($P = 6 \times 10^{-7}$); and (*v*) 41 oligodendrocyte-enriched genes, $\rho_{mh} = 0.65$ ($P = 7 \times 10^{-6}$) (57). Consistent with the enhancement of a meaningful signal, mouse–human correspondence increased as progressively more stringent quality-control criteria were applied to the mouse gene-expression data (*SI Appendix*, Fig. S9).

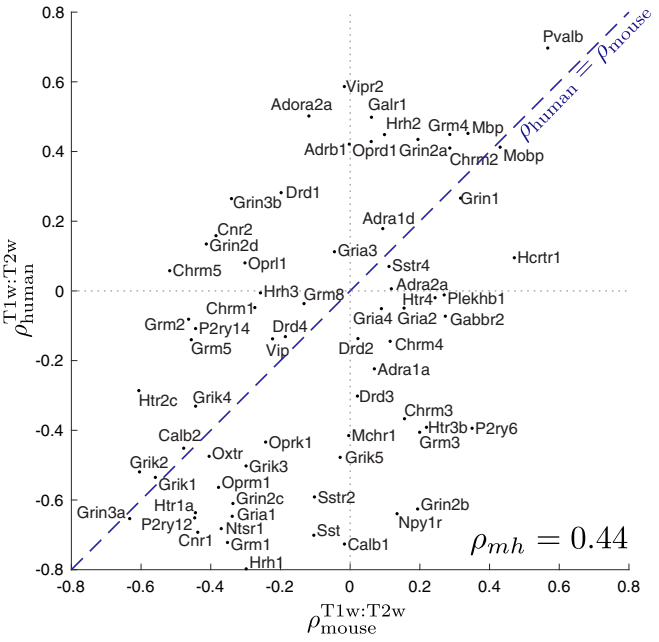

Fig. 5. Mouse–human consistency of T1w:T2w and transcriptional gradients of brain-related genes. We plot the correlation between T1w:T2w and transcription levels in mice, $\rho_{\text{mouse}}^{\text{T1w:T2w}}$ (horizontal axis), and humans, $\rho_{\text{human}}^{\text{T1w:T2w}}$ (vertical axis), for 70 brain-related genes. The equality line is shown as a dashed blue line. Transcriptional maps of key brain-related genes vary similarly with T1w:T2w in mouse and human cortex, $\rho_{mh} = 0.44$ ($P = 1 \times 10^{-4}$).

Discussion

Macroscale spatial variations in the makeup of cortical microcircuits may reflect a biological substrate of functional specialization that enables efficient processing and integration of diverse sensory information (5, 7, 10, 20, 21, 25) across multiple timescales (58–60). Here we show that these large-scale hierarchical gradients observed in macaque and human cortex (25) match those in mice, which display an underappreciated level of interareal heterogeneity. Circumventing the need to define an interspecies homology (61), we used the noninvasive MRI contrast map, T1w:T2w, as a common spatial reference for interspecies comparison; T1w:T2w varies similarly in both mouse and human cortex with the dominant cortical map of transcriptional variation (estimated using PCA) and with specific transcriptional maps of genes encoding synaptic receptors and neuronal cell types. Using high-resolution invasive measurements available in mice, we report additional connections between T1w:T2w and cell densities, laminar-specific gene expression, and interareal axonal connectivity. Our results provide more understanding of the anatomical underpinning of hierarchical functional specialization and demonstrate the usefulness of using noninvasive measurements like T1w:T2w to index large-scale gradients across species. While the complexity of cortical diversity clearly cannot be indexed by a single measurement like T1w:T2w, the covariation of diverse aspects of microcircuit architecture along a common spatial map, as well as its interspecies correspondence, supports the existence of stereotypical anatomical properties that support hierarchical specialization in mammalian brains.

The degree of interareal variation of microstructural properties in mice (8, 9) is far less pronounced than in the highly differentiated primate cortex (7, 10, 62). For example, in rhesus monkeys, the physiology and morphology of layer 3 pyramidal neurons (26) and glutamatergic synaptic structure (27) exhibit strong interareal differences between V1 and frontal cortex, properties that are strikingly homogeneous by comparison between homologous areas of mouse cortex. While the mouse cortex exhibits hierarchical feedforward–feedback projection patterns in specific (e.g., visual) processing streams (63),

with a corresponding variation in microstructure (64), interareal laminar projections across the whole cortex appear to be more stereotyped in macaques (65) than in mice (30). Different functional modules of the mouse cortex fit a hierarchical organization to differing extents, with a low hierarchy score for the prefrontal module (0.03) and higher scores for visual (0.33) and temporal (0.51) modules, where a maximum score of 1 corresponds to an ideal hierarchy (30). Across the whole cortex, mouse brain areas fit relatively poorly into a global hierarchical organization, attaining a hierarchy score of just 0.126, although this index is yet to be calculated in macaques, preventing direct interspecies comparison. Consistent with a lesser degree of differentiation in mouse cortex, here we report consistently weaker correlations of T1w:T2w with other spatial maps relative to macaques and humans, for hierarchical level ($\rho_{\mathrm{macaque}} = -0.76$, $\rho_{\mathrm{mouse}} = -0.29$), cytoarchitectural type ($\tau_{\mathrm{macaque}} = 0.87$, $\tau_{\mathrm{mouse}} = 0.51$), and the leading principal component of gene transcription ($|\rho_{\mathrm{mouse}}| = 0.53$, $|\rho_{\mathrm{human}}| = 0.81$) (25). A small number of genes exhibit mouse–human differences in the direction of their expression gradients with T1w:T2w (Fig. 5), but in most of these cases the correlation is weak in either mice or humans and may be attributable to measurement noise in the atlas-based expression data used here. However, our analysis flags candidate genes that further investigation may reveal to show robust mouse–human differences in the direction of expression gradients with T1w:T2w, including NMDA receptor signaling genes *Grin2b*/*GRIN2B* ($\rho_m = 0.19$, $\rho_h = -0.63$), *Grin2d*/*GRIN2D* ($\rho_m = -0.41$, $\rho_h = 0.13$), and *Grin3b*/*GRIN3B* ($\rho_m = -0.34$, $\rho_h = 0.26$).

As well as interspecies differences, our results also highlight an underappreciated spatial dimension of cortical specialization in mice that matches cortical gradients in primates. The consistency of transcriptional maps of 70 receptor subunit and cell-type marker genes with the common reference map, T1w:T2w, in mice and humans ($\rho_{mh} = 0.44$, $P = 1 \times 10^{-4}$) is striking given vastly different spatial scales and major differences in expression measurement between mice [high-throughput in situ hybridization (32)] and humans [microarray data from six postmortem subjects (56)]. In contrast to the findings above, in which we found a generally weaker relationship of cortical gradients to T1w:T2w in mice relative to primates, these transcriptional gradients were comparable in magnitude between the two species. A 2D projection of mouse cortical areas based on their transcriptional signatures across brain-expressed genes (Fig. 2*C*) distinguishes somatomotor, auditory, and visual processing streams from anterolateral and prefrontal areas and yields an organization analogous to parallel processing streams in low-dimensional embeddings of human fMRI correlation networks (18, 66).

T1w:T2w is commonly interpreted as a marker of gray-matter myelin content (45), although both T1- and T2-weighted images are sensitive to a wide range of microstructural properties (46). Our results provide transcriptional evidence for a connection between T1w:T2w and myelin (67), demonstrating a significant relationship with the expression of *Mobp* and other oligodendrocyte-enriched genes (which also display high mouse–human correspondence, $\rho_{mh} = 0.65$). Interpreting T1w:T2w as a marker of relative intracortical myelination is consistent with the increase in T1w:T2w across areas with increasing laminar differentiation, which is associated with myelin content (4, 5, 48). Axonal myelination improves transmission speeds (68) and prevents the formation of new synaptic connections (69, 70), properties that are consistent with the fast, "hard-wired" computations in heavily myelinated and eulaminar somatosensory areas relative to more plastic and adaptive agranular prefrontal areas (3, 5). While these diverse gradients may reflect associated differences in myelination, other gradients reported here cannot be linked straightforwardly to relative myelination levels, such as the strong transcriptional variation of *Grin3a* and *Calb2* with T1w:T2w. The convergence of multimodal cortical gradients may therefore reflect deeper organizational mechanisms acting in concert, perhaps through development (51). Our results are consistent with existing models of mammalian cortical organization based on systematic structural variation as a core organizing principle (48); in this context, the convergence of diverse gradients found here could be used to predict laminar patterns of interareal connectivity (30) that do not rely on a global hierarchical representation of cortical areas. To understand the functional importance of the dominant cortical gradient reported here, further work is needed to explain how characteristic differences in synaptic structure and inhibitory control may allow for more flexible behavior at the level of information processing within local microcircuits (3, 48).

As more is learned about how variations in cellular and synaptic microstructure shape functional specialization in the cortex, it will be important to complement this understanding with new mathematical models of brain dynamics that are properly constrained by the breadth and spatial detail of new datasets (29, 59, 71, 72). Such approaches will allow theory and experiment to develop in tandem, with physiologically constrained mathematical models making functional predictions that can be tested experimentally and used to refine the models. Understanding how individual cortical areas—each treated as a local computational unit (73) with distinctive dynamical properties—communicate coherently on a whole-brain scale may aid motivation for the next generation of brain-inspired machine-learning algorithms (74). Our findings offer guidance for the development of dynamical and functional models of large-scale cortical circuits in mammalian species.

Materials and Methods

A summary of our data and analysis methods is provided here, with additional details provided in *SI Appendix*. For all datasets considered, we retrieved values for each of 40 brain regions from the Allen Brain Reference Atlas Common Coordinate Framework (CCFv3) (33, 49), where possible. T1w:T2w data were obtained from the scalable brain atlas (53) in Waxholm space (75) and rescaled to 25-μm isotropic voxel spacing and normalized to CCFv3, as shown in *SI Appendix*, Figs. S1 and S2. Cell densities (/mm^3) of neurons, glia, excitatory cells, inhibitory cells, modulatory cells, astrocytes, oligodendrocytes, and microglia are from Erö et al. (40). Cell-count data are also from CUBIC-Atlas (39). Cytoarchitectonic classification of areas is from Goulas et al. (37). Mouse brain axonal connectivity weights were taken as normalized connection densities from the statistical model of Oh et al. (33). Interneuron cell densities by region and layer are from qBrain (29). Transcriptional maps (including for specific layers) are from the AMBA (32) and were filtered by applying stringent quality-control criteria to allow interpretable spatial maps for 4,181 genes. T1w:T2w correlations to gene transcriptional maps in human cortex are taken from an analysis of AHBA data (56) by Burt et al. (25).

ACKNOWLEDGMENTS. We thank Alex Fornito for his detailed and insightful comments on the manuscript. B.D.F. is supported by the National Health and Medical Research Council Grant 1089718. J.D.M. is supported by National Institute of Mental Health (NIMH) Grant R01MH112746. V.Z. is supported by the Swiss National Science Foundation Ambizione PZ00P3_173984. X.-J.W. is supported by NIMH Grant R01MH062349, Simons Collaborative Global Brain Program Grant 543057SPI, and Office of Naval Research Grant N00014-17-1-2041.

1. Charvet CJ, Finlay BL (2014) Evo-devo and the primate isocortex: The central organizing role of intrinsic gradients of neurogenesis. *Brain Behav Evol* 84:81–92.
2. Beul SF, Hilgetag CC (2015) Towards a "canonical" agranular cortical microcircuit. *Front Neuroanat* 8:7021.
3. Goulas A, Zilles K, Hilgetag CC (2018) Cortical gradients and laminar projections in mammals. *Trends Neurosci* 41:775–788.
4. Sanides F (1970) Functional architecture of motor and sensory cortices in primates in the light of a new concept of neocortex evolution. *The Primate Brain Advances*

in Primatology, eds Noback CR, Montagna W (Appleton-Century-Crofts Educational Division/Meredith Corporation, New York), pp 137–208.
5. García Cabezas MÁ, Joyce MKP, John YJ, Zikopoulos B, Barbas H (2017) Mirror trends of plasticity and stability indicators in primate prefrontal cortex. *Eur J Neurosci* 46:2392–2405.
6. Elston GN (2000) Pyramidal cells of the frontal lobe: All the more spinous to think with. *J Neurosci* 20:1–4.
7. Elston GN (2003) Cortex, cognition and the cell: New insights into the pyramidal neuron and prefrontal function. *Cereb Cortex* 13:1124–1138.
8. Ballesteros-Yáñez I, Benavides-Piccione R, Elston GN, Yuste R, DeFelipe J (2006) Density and morphology of dendritic spines in mouse neocortex. *Neuroscience* 138:403–409.
9. Benavides-Piccione R, Hamzei-Sichani F, Ballesteros-Yáñez I, DeFelipe J, Yuste R (2006) Dendritic size of pyramidal neurons differs among mouse cortical regions. *Cereb Cortex* 16:990–1001.
10. Elston GN, Fujita I (2014) Pyramidal cell development: Postnatal spinogenesis, dendritic growth, axon growth, and electrophysiology. *Front Neuroanat* 8:13644.
11. Sasaki T, Aoi H, Oga T, Fujita I, Ichinohe N (2014) Postnatal development of dendritic structure of layer III pyramidal neurons in the medial prefrontal cortex of marmoset. *Brain Struct Funct* 220:3245–3258.
12. Medalla M, Luebke JI (2015) Diversity of glutamatergic synaptic strength in lateral prefrontal versus primary visual cortices in the rhesus monkey. *J Neurosci* 35:112–127.
13. Palomero-Gallagher N, Zilles K (August 12, 2017) Cortical layers: Cyto-, myelo-, receptor- and synaptic architecture in human cortical areas. *NeuroImage*, 10.1016/j.neuroimage.2017.08.035.
14. Hof PR, et al. (1999) Cellular distribution of the calcium-binding proteins parvalbumin, calbindin, and calretinin in the neocortex of mammals: Phylogenetic and developmental patterns. *J Chem Neuroanat* 16:77–116.
15. Dombrowski SM, Hilgetag CC, Barbas H (2001) Quantitative architecture distinguishes prefrontal cortical systems in the rhesus monkey. *Cereb Cortex* 11:975–988.
16. Harris KD, Shepherd GMG (2015) The neocortical circuit: Themes and variations. *Nat Neurosci* 18:170–181.
17. Wagstyl K, Ronan L, Goodyer IM, Fletcher PC (2015) Cortical thickness gradients in structural hierarchies. *NeuroImage* 111:241–250.
18. Margulies DS, et al. (2016) Situating the default-mode network along a principal gradient of macroscale cortical organization. *Proc Natl Acad Sci USA* 113:12574–12579.
19. van den Heuvel MP, Yeo BTT (2017) A spotlight on bridging microscale and macroscale human brain architecture. *Neuron* 93:1248–1251.
20. Huntenburg JM, Bazin PL, Bazin PL, Margulies DS (2017) Large-scale gradients in human cortical organization. *TICS* 22:21–31.
21. Medalla M, Gilman JP, Wang JY, Luebke JI (2017) Strength and diversity of inhibitory signaling differentiates primate anterior cingulate from lateral prefrontal cortex. *J Neurosci* 37:4717–4734.
22. Mesulam MM (1998) From sensation to cognition. *Brain* 121:1013–1052.
23. Jones E, Powell T (1970) An anatomical study of converging sensory pathways within the cerebral cortex of the monkey. *Brain* 93:793–820.
24. Zilles K, Amunts K (2012) Segregation and wiring in the brain. *Science* 335:1582–1584.
25. Burt JB, et al. (2018) Hierarchy of transcriptomic specialization across human cortex captured by structural neuroimaging topography. *Nat Neurosci* 21:1251–1259.
26. Gilman JP, Medalla M, Luebke JI (2016) Area-specific features of pyramidal neurons—a comparative study in mouse and rhesus monkey. *Cereb Cortex* 27:2078–2094.
27. Hsu A, Luebke JI, Medalla M (2017) Comparative ultrastructural features of excitatory synapses in the visual and frontal cortices of the adult mouse and monkey. *J Comparat Neurol* 525:2175–2191.
28. Luebke JI (2017) Pyramidal neurons are not generalizable building blocks of cortical networks. *Front Neuroanat* 11:13644.
29. Kim Y, et al. (2017) Brain-wide maps reveal stereotyped cell-type-based cortical architecture and subcortical sexual dimorphism. *Cell* 171:456–469.e22.
30. Harris JA, et al. (2018) The organization of intracortical connections by layer and cell class in the mouse brain. bioRxiv:292961. Preprint, posted April 18, 2018.
31. Fürth D, et al. (2017) An interactive framework for whole-brain maps at cellular resolution. *Nat Neurosci* 21:139–149.
32. Lein E, et al. (2006) Genome-wide atlas of gene expression in the adult mouse brain. *Nature* 445:168–176.
33. Oh SW, et al. (2014) A mesoscale connectome of the mouse brain. *Nature* 508: 207–214.
34. Zingg B, et al. (2014) Neural networks of the mouse neocortex. *Cell* 156:1096–1111.
35. Hintiryan H, et al. (2016) The mouse cortico-striatal projectome. *Nat Neurosci* 19:1100–1114.
36. Gămănuţ R, et al. (2018) The mouse cortical connectome, characterized by an ultradense cortical graph, maintains specificity by distinct connectivity profiles. *Neuron* 97:698–715.
37. Goulas A, Uylings HBM, Hilgetag CC (2016) Principles of ipsilateral and contralateral cortico-cortical connectivity in the mouse. *Brain Struct Funct* 252:1–15.
38. Herculano-Houzel S, Watson CR, Paxinos G (2013) Distribution of neurons in functional areas of the mouse cerebral cortex reveals quantitatively different cortical zones. *Front Neuroanat* 7:35.
39. Murakami TC, et al. (2018) A three-dimensional single-cell-resolution whole-brain atlas using CUBIC-X expansion microscopy and tissue clearing. *Nat Neurosci* 21:625–637.
40. Erö C, Gewaltig MO, Keller D, Markram H (2018) A cell atlas for the mouse brain. *Front Neuroinf* 12:e17727.
41. Zerbi V, Grandjean J, Rudin M, Wenderoth N (2015) Mapping the mouse brain with rs-fMRI: An optimized pipeline for functional network identification. *NeuroImage* 123:11–21.
42. Sethi SS, Zerbi V, Wenderoth N, Fornito A, Fulcher BD (2017) Structural connectome topology relates to regional BOLD signal dynamics in the mouse brain. *Chaos* 27:047405.
43. Grandjean J, Zerbi V, Balsters J, Wenderoth N, Rudina M (2017) The structural basis of large-scale functional connectivity in the mouse. *J Neurosci* 37:8092–8101.
44. Fulcher BD, Fornito A (2016) A transcriptional signature of hub connectivity in the mouse connectome. *Proc Natl Acad Sci USA* 113:1435–1440.
45. Glasser MF, Van Essen DC (2011) Mapping human cortical areas in vivo based on myelin content as revealed by T1- and T2-weighted MRI. *J Neurosci* 31:11597–11616.
46. Lorio S, et al. (2016) Neurobiological origin of spurious brain morphological changes: A quantitative MRI study. *Hum Brain Map* 37:1801–1815.
47. Markov NT, et al. (2013) Cortical high-density counterstream architectures. *Science* 342:1238406.
48. Barbas H (2015) General cortical and special prefrontal connections: Principles from structure to function. *Annu Rev Neurosci* 38:269–289.
49. Dong HW (2008) *The Allen Reference Atlas: A Digital Color Brain Atlas of the C57Bl/6J Male Mouse* (Wiley, Hoboken, NJ).
50. Benjamini Y, Hochberg Y (1995) Controlling the false discovery rate: A practical and powerful approach to multiple testing. *J R Stat Soc B* 57:289–300.
51. Chomiak T, Hu B (2017) Mechanisms of hierarchical cortical maturation. *Front Cell Neurosci* 11:150–158.
52. Finger JH, et al. (2017) The mouse gene expression database (GXD): 2017 update. *Nucleic Acid Res* 45:D730–D736.
53. Bakker R, Tiesinga P, Kötter R (2015) The scalable brain atlas: Instant web-based access to public brain atlases and related content. *NeuroInf* 13:353–366.
54. Janušonis S (2017) A receptor-based analysis of local ecosystems in the human brain. *BMC Neurosci.* 18:551.
55. Ilin A, Raiko T (2010) Practical approaches to principal component analysis in the presence of missing values. *J Mach Learn Res* 11:1957–2000.
56. Hawrylycz MJ, et al. (2012) An anatomically comprehensive atlas of the adult human brain transcriptome. *Nature* 489:391–399.
57. Cahoy JD, et al. (2008) A transcriptome database for astrocytes, neurons, and oligodendrocytes: A new resource for understanding brain development and function. *J Neurosci* 28:264–278.
58. Murray JD, et al. (2014) A hierarchy of intrinsic timescales across primate cortex. *Nat Neurosci* 17:1661–1663.
59. Chaudhuri R, Knoblauch K, Gariel MA, Kennedy H, Wang XJ (2015) A large-scale circuit mechanism for hierarchical dynamical processing in the primate cortex. *Neuron* 88:419–431.
60. Duarte R, Seeholzer A, Zilles K, Morrison A (2017) Synaptic patterning and the timescales of cortical dynamics. *Curr Opin Neurobiol* 43:156–165.
61. Tan PPC, French L, Pavlidis P (2013) Neuron-enriched gene expression patterns are regionally anti-correlated with oligodendrocyte-enriched patterns in the adult mouse and human brain. *Front Neurosci* 7:5.
62. Charvet CJ, Cahalane DJ, Finlay BL (2015) Systematic, cross-cortex variation in neuron numbers in rodents and primates. *Cereb Cortex* 25:147–160.
63. D'Souza RD, Burkhalter A (2017) A laminar organization for selective cortico-cortical communication. *Front Neuroanat* 11:411.
64. D'Souza RD, Meier AM, Bista P, Wang Q, Burkhalter A (2016) Recruitment of inhibition and excitation across mouse visual cortex depends on the hierarchy of interconnecting areas. *eLife* 5:1025.
65. Markov NT, et al. (2012) A weighted and directed interareal connectivity matrix for macaque cerebral cortex. *Cereb Cortex* 24:17–36.
66. Guell X, Schmahmann JD, Gabrieli JD, Ghosh SS (2018) Functional gradients of the cerebellum. *eLife* 7:568.
67. Ritchie J, Pantazatos SP, French L (2018) Transcriptomic characterization of MRI contrast, focused on the T1-w/T2-w ratio in the cerebral cortex. *NeuroImage* 174:504–517.
68. Micheva KD, et al. (2016) A large fraction of neocortical myelin ensheathes axons of local inhibitory neurons. *eLife* 5:e15784.
69. Braitenberg V (1962) A note on myeloarchitectonics. *J Comp Neurol* 118:141–156.
70. Huntenburg JM, et al. (2017) A systematic relationship between functional connectivity and intracortical myelin in the human cerebral cortex. *Cereb Cortex* 27:981–997.
71. Demirtas M, et al. (February 7, 2019) Hierarchical heterogeneity across human cortex shapes large-scale neural dynamics. *Neuron*, 10.1016/j.neuron.2019.01.017.
72. Murray JD, Demirtas M, Anticevic A (2018) Biophysical modeling of large-scale brain dynamics and applications for computational psychiatry. *Biol Psychiatry Cog Neurosci Neuroimag* 3:777–787.
73. Douglas RJ, Martin KAC (2007) Mapping the matrix: The ways of neocortex. *Neuron* 56:226–238.
74. Marblestone AH, Wayne G, Kording KP (2016) Toward an integration of deep learning and neuroscience. *Front Comput Neurosci* 10:406.
75. Johnson GA, et al. (2010) Waxholm space: An image-based reference for coordinating mouse brain research. *NeuroImage* 53:365–372.